Materials Horizons

ROYAL SOCIETY OF CHEMISTRY

COMMUNICATION

View Article Online
View Journal | View Issue

Check for updates

Cite this: *Mater. Horiz.*, 2023, 10, 859

Received 17th October 2022,
Accepted 13th December 2022

DOI: 10.1039/d2mh01289h

rsc.li/materials-horizons

Published on 19 2022. Downloaded on 16.10.2025 08:37:42.

A self-healing polymerized-ionic-liquid-based polymer electrolyte enables a long lifespan and dendrite-free solid-state Li metal batteries at room temperature†

Xiujing Lin,[a] Shiyuan Xu,[a] Yuqi Tong,[a] Xinshuang Liu,[a] Zeyu Liu,[a] Pan Li,[a] Ruiqing Liu,[a] Xiaomiao Feng,[a] Li Shi*[a] and Yanwen Ma*[ab]

The implementation of high-safety Li metal batteries (LMBs) needs more stable and safer electrolytes. The solid-state electrolytes (SSEs) with their advantageous properties stand out for this purpose. However, low Li/electrolyte interfacial instability and uncontrolled Li dendrites growth trigger unceasing breakage of the solid electrolyte interphase (SEI), leading to fast capacity degradation. In response to these shortcomings, a new type of polymer electrolyte with self-healing capacity is introduced by grafting ionic liquid chain units into the backbones of polymers, which inherits the chemical inertness against the Li anode, allowing high Li^+ transport, wide electrochemical window, and self-healing traits. Benefiting from the strong external H-bonding interactions, the obtained polymer electrolyte can spontaneously reconstruct dendrite-induced defects and fatigue crack growth at the Li/electrolyte interface, and, in turn, help tailor Li deposition. Owing to the resilient Li/electrolyte interface and dendrite-free Li plating, the equipped Li|LFP batteries display a high initial specific capacity of 134.7 mA h g^{-1}, rendering a capacity retention of 91.2% after 206 cycles at room temperature. The new polymer electrolyte will undoubtedly bring inspiration for developing practical LMBs with highly improved safety and interfacial stability.

New concepts

Low Li/electrolyte interfacial instability and uncontrolled growth of lithium dendrites trigger unceasing breakage of the solid electrolyte interphase (SEI) and impede the practical application of solid-state electrolytes. Herein, we introduce a self-healing polymerized-ionic-liquid-based polymer electrolyte by grafting ionic liquid chain units into the backbones of polymers. With this strategy, the obtained polymer inherits the dimensional stability and mechanical durability of polymers, while retaining the traits of ionic liquids. In response to the designability of ionic liquid monomers, specific groups conducive to hydrogen bonding are adopted to impart the self-healing capability to the polymer. This characteristic allows it to spontaneously reconstruct dendrite-induced defects at the Li/electrolyte interface, and, in turn, tailor Li deposition. With the synthesized polymer electrolyte, the solid-state Li|$LiFePO_4$ batteries deliver the best in-class cyclical stability at room temperature.

1. Introduction

Given the high specific capacity, low redox potential, and low atomic weight, the Li metal anodes-based secondary batteries have long remained on research agendas.[1,2] Unfortunately, the safety hazards associated with the flammable and leaky organic liquid electrolytes (OLE) utilized in conventional Li metal batteries (LMBs) impede their large-scale applications. Moreover, the direct parasitic reaction between organic liquid electrolytes and active Li anodes depletes the electrolytes, thicken the electrolyte/anode interphase, and ultimately brings about premature battery failure. Likewise, the uncontrolled Li dendritic generation throughout the cycling process may pierce the brittle separator, inducing internal short circuits and battery failure.[2–9]

To address such challenges, a variety of strategies, including flame-retardant additives, artificial *in/ex situ* solid electrolyte interphase (SEI), and the design of structured solid-state electrolytes (SSEs), have been utilized.[10,11] As an alternative to the organic liquid electrolyte, the SSE is considered more promising for safe energy storage owing to its inherent non-flammability and robust mechanical properties, which plays a pivotal role in restraining Li dendrites. Generally, SSEs can be mainly divided into two major types: inorganic ion-conducting ceramics and organic polymers (namely solid-state polymer electrolytes (SPEs)).[9–12]

[a] *Key Laboratory for Organic Electronics and Information Displays (KLOEID) & Institute of Advanced Materials (IAM), Jiangsu Key Laboratory for Biosensors, Jiangsu National Synergetic Innovation Center for Advanced Materials (SICAM), Nanjing University of Posts and Telecommunications, Nanjing, Jiangsu 210023, China. E-mail: iamlshi@njupt.edu.cn, iamywma@njupt.edu.cn*

[b] *Suzhou Vocational Institute of Industrial Technology, 1 Zhineng Avenue, Suzhou International Education Park, Suzhou 215104, China*

† Electronic supplementary information (ESI) available. See DOI: https://doi.org/10.1039/d2mh01289h

Published on 19 2022. Downloaded on 16.10.2025 08:37:42.

Compared with inorganic SSEs, SPEs exhibit overwhelming advantages in flexibility and can retain relatively close adhesion to Li anodes during cycling, which alleviates void generation at the electrolyte/anode interface. Polymer matrices, including poly(methyl methacrylate) (PMMA), poly(ethylene oxide) (PEO), poly(ethylene glycol) diacrylate (PEGDA), polyacrylonitrile (PAN), poly(vinylidene fluoride)-*co*-hexafluoropropylene (PVDF-HFP) and so on have been investigated to date.[13–16] However, all of these polymers show inadequate room-temperature ionic conductivity to enable long-term cycling. Incorporating plasticizers, such as carbonates, esters, ethers, and ionic liquids into polymer electrolytes, is effective in elevating ionic conductivity at ambient temperature, while maintaining the toughness of polymers. Ionic liquids (ILs), which are composed of organic cations and inorganic or organic anions, have rekindled an interest due to their unique properties, such as incombustibility, non-volatility, high ionic conductivity, and high thermal/electrochemical consistency.[17–23] Nevertheless, the adoption of ILs always sacrifices the mechanical capacities of polymers, such as strength and stretchability.

With the above consideration in mind, we reasoned that grafting ionic liquid chain units into the backbones of polymers would inherit the dimensional stability and mechanical durability of polymers without losing the traits of ILs. Based on the designability of ILs, designing of rational molecular structure, *e.g.* adopting a specific group conducive to hydrogen bonding, is an efficacious strategy to endow the polymers with unique properties, such as thermal stability, hydrophobicity, and self-healing. Particularly for remedying the dendrite-induced defects and fatigue crack growth at the Li/electrolyte interface, a self-healing polymer can eliminate crack propagation spontaneously, reduce explosion hazard, and thus, prolong the lifespan of LMBs.[24] Arumugam *et al.* explored a self-healing polymer electrolyte with 1-allyl-3-methylimidazolium bis(trifluoromethanesulfonyl)imide (AMIMTFSI) and MMA as backbone and EMIFTFSI as the ionic liquids filler. Benefitting from the quick self-healing ability, the solid polymer electrolyte exhibits high compatibility with Li metal.[25] Guo and co-workers designed a polymer electrolyte by applying 2-(3-(6-methyl-4-oxo-1,4-dihydropyrimidin-2-yl)ureido) ethyl methacrylate (UPyMA) as the self-healing units, which certainly contributed to the establishment of compact Li/electrolyte interface, and therefore, aided in repairing interfacial flaws.[26] Through two PEO networks crosslinked by reversible disulfide and imine bonds, the Zhang group synthesized a self-healable solid polymer electrolyte. The Li|$LiFePO_4$ batteries assembled based on the electrolyte described above deliver a capacity retention of 88.4% over 300 cycles.[27]

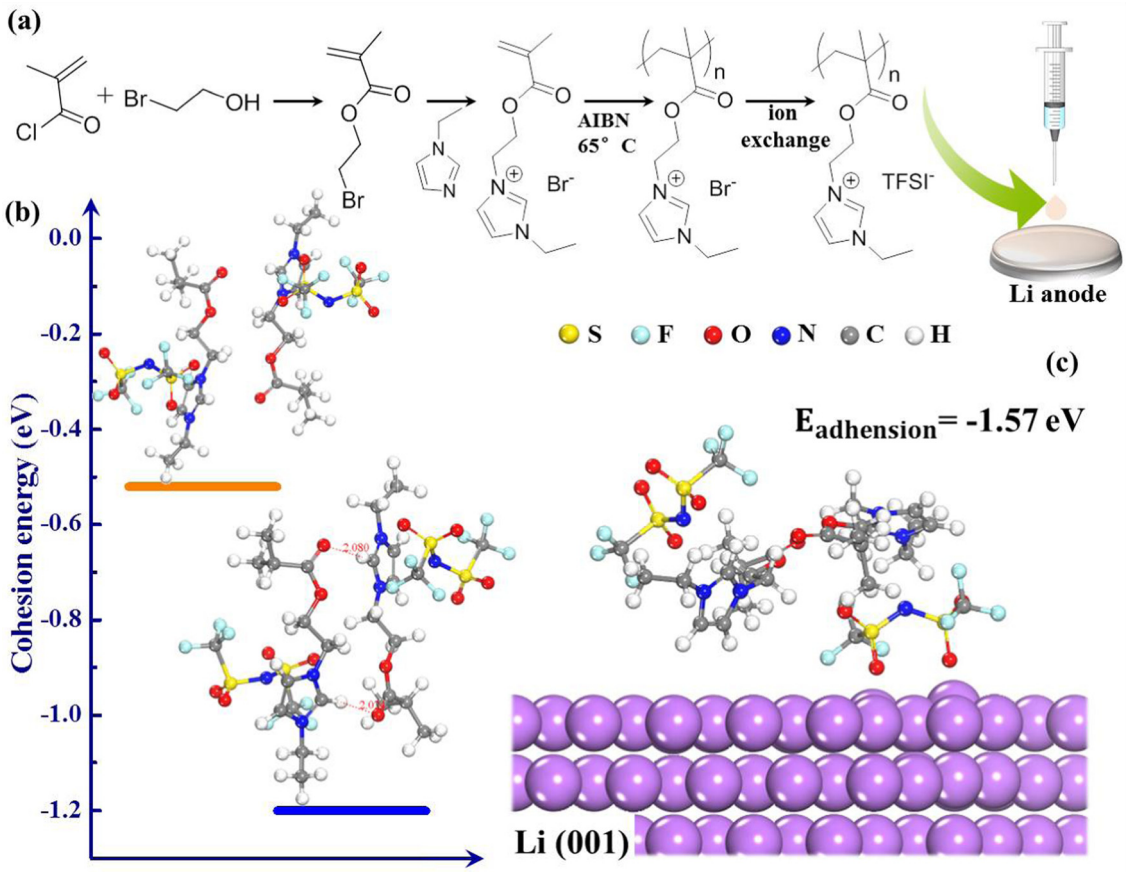

Fig. 1 (a) Schematic representation of the synthesis of PIL, (b) external H-bonding interactions between the carbonyl oxygen and imidazolium cations, (c) representation of the interaction of PIL and Li anode.

 This journal is © The Royal Society of Chemistry 2023

Published on 19 2022. Downloaded on 16.10.2025 08:37:42.

In this work, we introduce a new type of polymer electrolyte by grafting ionic liquid chain units ($EMIM^+$) into the backbones of polymers (PMMA) as presented in Fig. 1(a). From the design perspective, PMMA is used as the matrix of electrolyte because of its chemical stability towards Li, which endows the novel polymer electrolyte with wide electrochemical window.[28] The $EMIM^+$ facilitates superior cationic solvation and serves as an H-bonding donor, which could generate hydrogen bonds with oxygen-containing groups of PMMA (Fig. 1(b)),[29,30] making the polymer compatible with high Li^+ transport and fast self-healing ability. The external H-bonding interactions can spontaneously reconstruct dendrite-induced defects and fatigue crack growth at the Li/electrolyte interface, thus playing a constructive role in Li dendrite suppression. These peculiarities endow polymerized-ionic-liquid (PIL)-based LMBs with remarkable room-temperature cycling performance, presenting a capacity retention of 91.2% over 206 cycles at 0.5 °C. The self-healing polymer electrolyte provides the inspiration to develop practical LMBs with improved safety and interfacial stability.

2. Results and discussion

The target polymerized-ionic-liquid-based polymer of poly(1-ethyl-3-(2-methacryloyloxy ethyl) imidazolium bis(trifluoromethylsulphonyl)imide) (PEMEImTFSI) was synthesized by reacting *N*-ethylimidazole with 2-bromoethyl methacrylate, followed by polymerization triggered by AIBN and an anion exchange with $TFSI^-$.[31,32] Measurements with ^1H and ^{13}C NMR were used to confirm the backbone structure of EMEImBr monomers (Fig. 2(a) and (b)). The synthesis of PIL was completed by using azobisisobutyronitrile (AIBN) at 65 °C *via* free radical polymerization of C=C bonds on EMEImBr monomers. Fourier-transform infrared spectra (FTIR) measurements are shown in Fig. 2(c), which validate the polymerization of EMEImBr monomers. The peak around 1636 cm^{-1} in EMEImBr monomers corresponds to the stretching of C=C,[33,34] and it vanishes after polymerization, suggesting successful polymerization.

The top-view scanning electron microscopy (SEM) image of the PIL electrolyte (Fig. 3(a)) displays a smooth, flat surface and a homogeneous membrane without phase segregation. Fig. 3(b) shows that the transparent polymer electrolyte membrane can spontaneously self-heal within 3 h after being cut at room temperature; this healing is motivated by the external H-bond interactions. First-principles density functional theory (DFT) demonstrates that intermolecular H-bonding interaction occurs between C–H of the imidazolium ring and the oxygen atom of the carbonyl group (Fig. 1(b)). According to previous literature, H^2, H^4, and H^5 protons of imidazolium rings are H-bonding donors, which generate a hydrogen bond with other molecules, and thus, account for fast self-healing ability.[30] Furthermore, the high interfacial adhesive energy at the interface between the Li anode and PIL membrane also improves the self-healing capacity (Fig. 1(c)).

To evaluate the thermal stability of the PIL membrane, thermogravimetric analysis (TGA) was conducted. The membrane exhibits thermal endurance up to 190 °C (Fig. 3(c)), which is superior to conventional organic liquid electrolytes with points of flammability near ambient temperature.[22,35] The electrochemical stability of the PIL

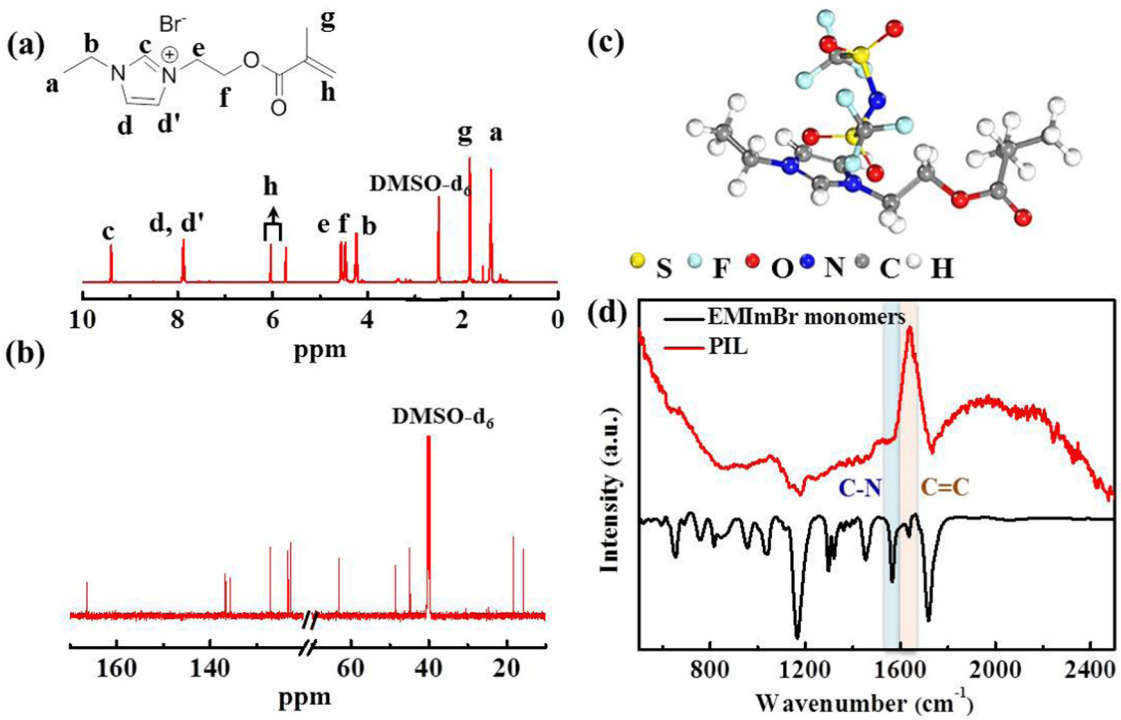

Fig. 2 (a) ^1H NMR and (b) ^{13}C NMR spectra of EMEImBr monomer, (c) chemical configuration of PIL, (d) FTIR spectra of EMEImBr monomer and PIL polymer matrix.

Published on 19 2022. Downloaded on 16.10.2025 08:37:42.

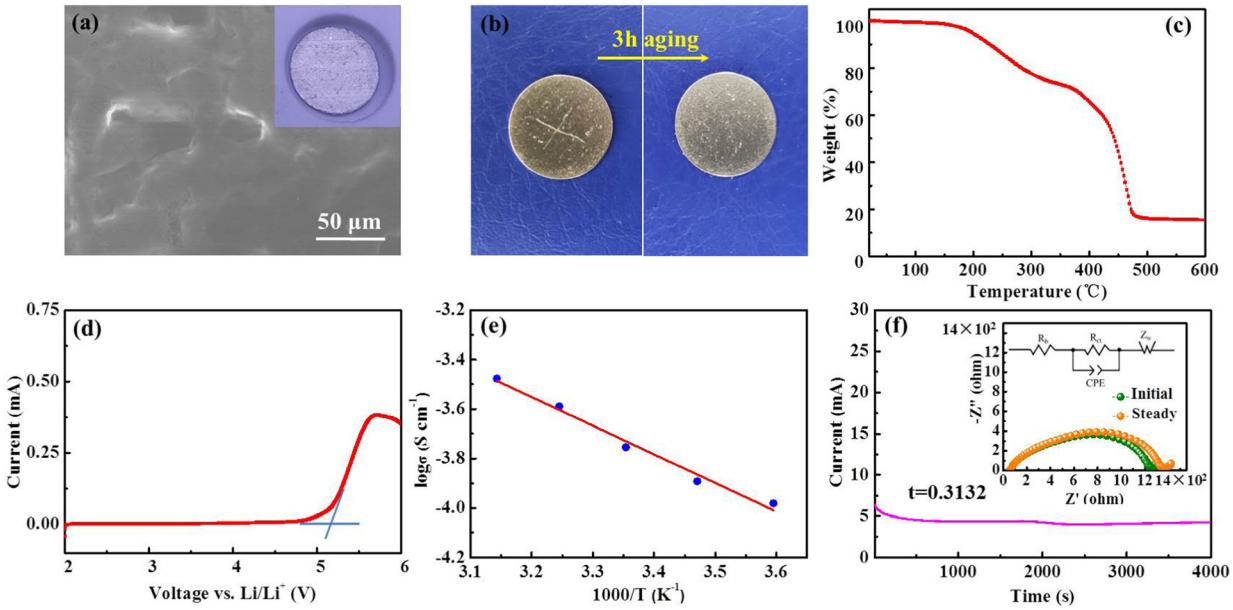

Fig. 3 (a) SEM image of PIL membrane, inset showing the optical photo of Li/PIL; (b) digital photos of the self-healing process of PIL membrane; (c) TGA curves and (d) LSV profile of PIL membrane; (e) temperature dependence of the ionic conductivity; (f) Li^+ transference number of PIL membrane, inset showing the Nyquist plots before and after polarization potential.

electrolyte was investigated by the linear sweep voltammetry (LSV) measurement. According to the results in Fig. 3(d), the PIL electrolyte does not encounter electrochemical oxidation until 5.2 V *vs.* Li/Li^+. The temperature effects on the ionic conductivity of the PIL electrolyte are further illustrated in Fig. 3(e). The plots of $\log \sigma$ *versus* $1000/T$ exhibit a linear relationship, which could be well fitted by the Arrhenius equation below:

$$\sigma(T) = A \exp\left(-\frac{E_a}{\kappa T}\right)$$

where σ, κ, T, and A refer to the ion conductivity, Boltzmann constant, absolute temperature, and pre-exponential factor, respectively. The activation energy E_a of the polymer electrolyte is calculated to be 0.23 eV, indicating a low activation barrier for the ion transport.[26,36–38] An ionic conductivity value of 1.76×10^{-4} S cm^{-1} is obtained by the PIL electrolyte at the room temperature (25 °C). The Li^+ transference number (t_{Li^+}) is another significant evaluation criterion. Fig. 3(f) depicts the chronoamperometry profiles and resistance values before and after applying a polarization potential of 10 mV. The t_{Li^+} of the PIL electrolyte is calculated to be 0.31, which is higher than the typical polymer solid electrolytes (*e.g.*, t_{Li^+} for PEO-based SPE is ≈ 0.2[22,39]). The enhancement in t_{Li^+} would lie in the weak affinity interaction between Li^+ and the synthesized polymer chains repelled by imidazolium cation, compared with that of PEO-based SPE, which improves Li^+ transport to a great extent.

Typically, solid polymer electrolyte membranes were achieved by the solution casting method, involving mass input of organic solvents unfriendly to the environment. The solvent-free hot-pressing technology was put forward to fabricate the crosslinked PEO-based electrolyte, which required additional investment in hot-pressing machines. However, they both belong to *ex situ* processing methods and could not adhere to the electrode during long-time cycling. An ideal electrolyte membrane depends not only on the novel polymer hosts with high ionic conductivity and electrochemical compatibility towards high-voltage cathodes, but also on the improvement of processing technology. Herein, we fabricate the PIL membrane *via* an *in situ* technique that enables close contact and affinity for anodic electrodes. For comparison, the Li|LFP ($Li|LiFePO_4$) batteries with freestanding PIL electrolyte membrane and PIL membrane fabricated on the cathode were assembled and detected in the same condition (Fig. S1, ESI†). In stark contrast to PIL coating on the Li anode, the battery with PIL coating on the cathode encounters battery failure during the 7th cycle. For the battery with a freestanding PIL membrane, capacities above the theoretical value are observed in dozens of circulations associated with electrolyte decomposition, SEI generation,[40] followed by a drastic fluctuation in capacity and Coulombic efficiency, manifesting the unstable interface. A galvanostatic intermittent titration technique (GITT) was applied on the Li|LFP batteries with PIL coating on the Li anode at 0.1C to further investigate the Li/electrolyte interface. As presented in Fig. 4(a), a charge/discharge voltage gap of ~0.12 V between the charge plateau and discharge plateau is achieved, which stands almost still in the following circulation, indicating a stable electrode/electrolyte interface.

Beyond the appropriate ionic conduction, interfacial stability is extraordinarily crucial for Li^+ distribution and electrodeposition behavior, which in turn, influences long-term battery operation. A comparative investigation of galvanostatic polarization in Li|Li symmetric batteries was conducted to assess Li stripping/plating reversibility between PIL and organic liquid electrolyte (1 M $LiPF_6$ in EC/DEC/DMC), whereby

 This journal is © The Royal Society of Chemistry 2023

Published on 19 2022. Downloaded on 16.10.2025 08:37:42.

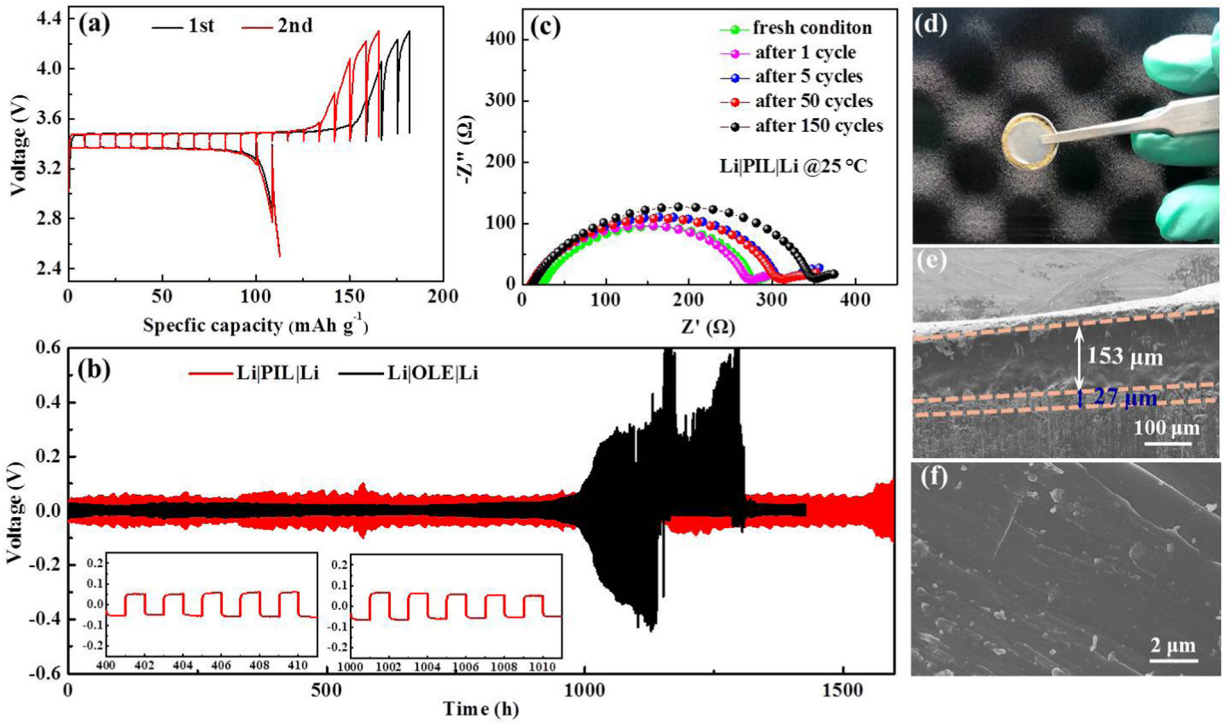

Fig. 4 (a) GITT curves of Li|LFP batteries with PIL membrane; (b) galvanostatic cycling performance of Li symmetrical battery, insets: partially enlarged images at a different time; (c) Nyquist plots of the symmetric Li battery with PIL membrane at various cycles; (d) digital photo of systematic battery after cycling; (e) cross-sectional SEM image of the Li|PIL|LFP battery after cycling; (f) top-view SEM image of the Li anode with PIL electrolyte after cycling.

1 h charge and discharge intervals under fixed currents were employed. The voltage response over time of the symmetric battery containing PIL and OLE was continuously detected at 0.05 mA cm^{-2} with 1 h interval per half cycle as presented in Fig. 4(b). The battery displays stationary Li plating/stripping behavior for more than 1600 h, accompanied by only a slight increase in the overpotential after 1500 h, which relates with the mild diminution in the contact surface between Li anode and PIL due to void formation. The voltage profiles in the insets indicate fluid Li plating/stripping with no observable phenomenon of the micro-short circuit, which leads to a sudden change in the voltage and distortion of the voltage curves.[22,36,41–43] Meanwhile, the battery cycles stably to 0.2 mA cm^{-2} in tests at step-varied currents, and the overpotential falls to 0.004 V, when the current density is restored to 0.01 mA cm^{-2} (Fig. S2, ESI†). The PIL-based symmetric battery exhibits good interfacial stability between Li foils and PIL electrolytes, while presenting high endurance against uneven Li deposition. The point is further validated by electrochemical impedance spectroscopy (EIS) results and SEM data in Fig. 4(c)–(f). As shown in Fig. 4(c), the battery with a PIL membrane delivers a slightly increasing interfacial resistance along with the prolonged cycling number at the beginning, which negligibly varies in the subsequent 40 cycles, indicating the robust contact between the PIL membrane and Li foils throughout the cycling process.[34] In terms of the morphology of cycled Li anodes, a truly smooth and flat surface is monitored by adopting PIL electrolyte, with no sign of rough Li dendrites, confirming uniform Li depositing/plating (Fig. 4(f)). The optical photograph and cross-sectional SEM image (Fig. 4(d) and (e)) show the PIL membrane maintains close contact with the Li anode, and a thin uniform Li plating layer with the thickness of ~27 μm are found along the Li anode. Inversely, massive Li dendrites emerge on the Li anode after long-time cycling, which may pierce into the PP separator for Li|OLE|Li battery, leading to a complete short-circuit (Fig. S2, ESI†).

To gain further insight into the inhibition mechanism of Li dendrites by PIL membrane, X-ray photoelectric spectroscopy (XPS) was introduced to further analyze the chemical composition of the interphase layer on the cycled Li anode. The results in Fig. 5(a) show that the F 1s spectrum is composed of Li–F peak (684.2 eV), C–F peak (686.8 eV), and S–F (688.0 eV),[22] displaying a high F content of 33.14% in the SEI layer. As the decomposition product of $TFSI^-$ anions, the SEI layer with rich LiF not only facilitates the formation of a stabilized interphase, but also induces dendrite-free Li plating owing to its ultrahigh mechanical strength and facile interfacial Li^+ ion transport.[36,44–46] Given the high reactivity of Li anodes, in-depth XPS measurements were also performed on the PIL membrane after cycling. Depth profiles of representative elements (Fig. 5(b)) demonstrate a mesophase layer with a thickness of 20 nm, which may contribute to stabilizing the Li/electrolyte interface.[2,14,47–50] Ordinarily, flaws at the Li/solid-state electrolyte interface result in uneven Li deposition and void formation, deteriorating the Li dendrites generation. As illustrated in Fig. 5(c), benefitting from the self-healing

Published on 19 2022. Downloaded on 16.10.2025 08:37:42.

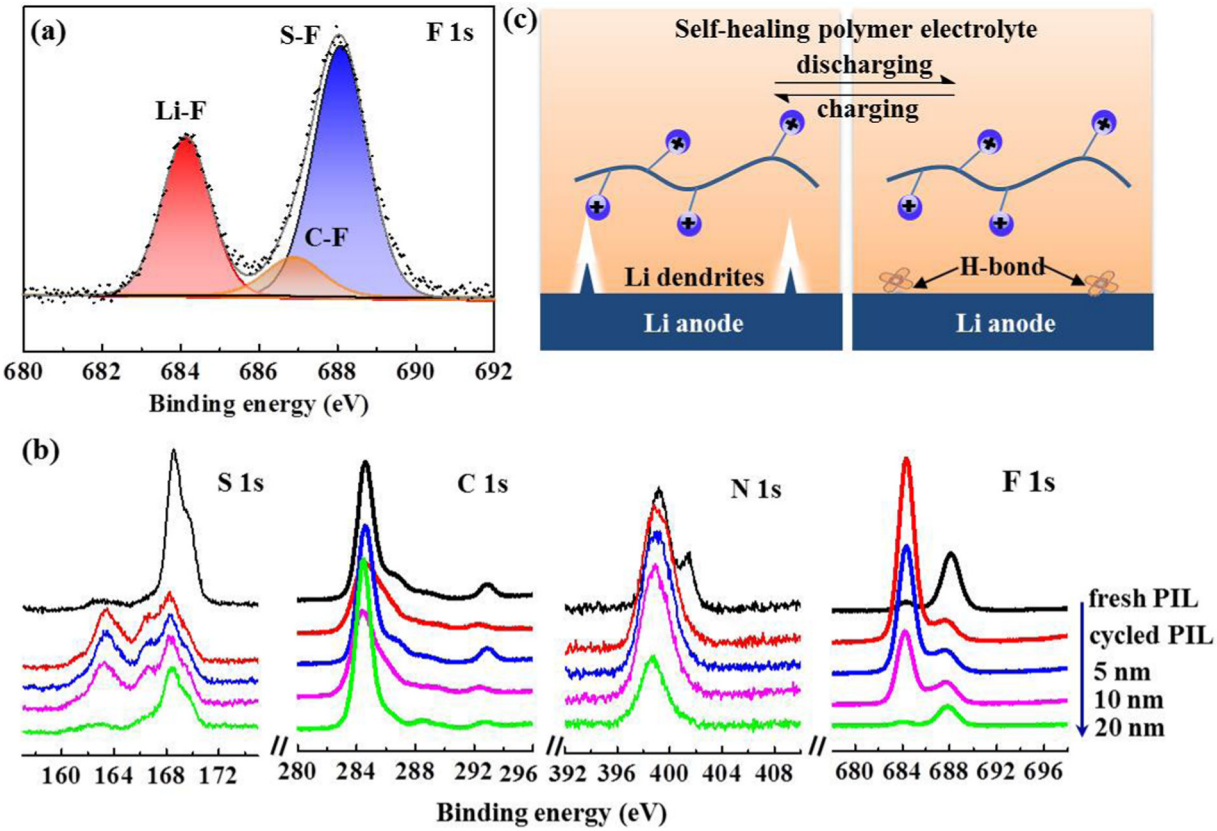

Fig. 5 (a) XPS spectra of F 1s revealing the surface chemistry of cycled Li anode with PIL electrolyte; (b) in-depth XPS spectra for the PIL electrolyte after cycling; (c) schematic illustration presenting the inhibition mechanism of Li dendrites in the self-healing electrolyte.

peculiarity, the novel polymer electrolyte not only remains an integrated Li/electrolyte interface, but also spontaneously remedies dendrite-induced voids at the interface, eliminating crack extension and enabling homogenous Li ionic flux.[26,36]

The polymerization degree has a profound impact on the features of PIL electrolytes. A high polymerization degree invests PIL electrolytes with mechanical properties at the cost of ion conductivity. Striking a balance between the two is crucially important. Table S1 (ESI†) summarizes the weight average molecular weight (M_w), number average molecular weight (M_n), and corresponding polydispersity indexes (M_w/M_n) of PIL electrolytes, respectively. Comparison of the diverse molecular weights formed in our synthesis implies that PIL-2 polymer with M_w of 28.418 kDa delivers superior cycling performance (Fig. 6(a)). In detail, an initial discharge specific capacity of 134.7 mA h g^{-1} is displayed by Li|PIL-2|LFP batteries at room temperature and 0.5C, which slowly fades to 122.9 mA h g^{-1} after 206 cycles, corresponding to an outstanding capacity retention of 91.2%. According to the typical voltage profiles, the battery shows high levels of reversibility and approximately flat charge/discharge plateaus at 3.54/3.31 V for 206 cycles, associating with the Li/Li^+ redox behavior of $LiFePO_4$ (Fig. 6(b)). For the batteries with other PIL polymers, a dramatic capacity decay is observed and a relatively lower discharge specific capacity of ~100 mA h g^{-1} is obtained at the end of 150 cycles. A polymer electrolyte membrane consisting of PMMA and EMIMTFSI precursors used to create our PIL polymers is fabricated by the conventional solution-casting method. The results listed in ESI,† Table S2 manifest the non-grafting PMMA/EMIMTFSI electrolyte encounters dramatic capacity fading in the first few circulations. It can be concluded that grafting $EMIM^+$ into the backbones of PMMA polymer exerts positive effects rather than compromising expediting Li stripping/plating processes. When cycling at 0.2C, the discharge specific capacity maintains 118.9 and 90.4 mA h g^{-1}, rendering capacity retention of 88.9% and 67.6% after 200 and 392 cycles, respectively (Fig. 6(c)). In terming of the charge/discharge curves (Fig. S3, ESI†), the battery with PIL membrane presents an extremely flat charge/discharge platform of 3.57/3.32 V. Nevertheless, the voltage gap displays a slightly increasing tendency starting from the 200th cycle. The rate capability of PIL-based Li|LFP batteries was evaluated from 0.1C to 1C at room temperature, as presented in Fig. 6(d). The reversible capacities of 148.9, 144.5, 131.7, and 104.6 mA h g^{-1} are achieved as the current density boosting from 0.1C to 1C. When the current density restores to 0.2C, the capacity recuperates to 124.5 mA h g^{-1}, accounting for 86.2% of the original capacity, validating the relative stability and robustness of this battery system.

A typical polymer electrolyte membrane not only serves as an ion conductor, but also functions as a separator sandwiching between the cathode and anode to avoid direct contact between

 This journal is © The Royal Society of Chemistry 2023

Published on 19 2022. Downloaded on 16.10.2025 08:37:42.

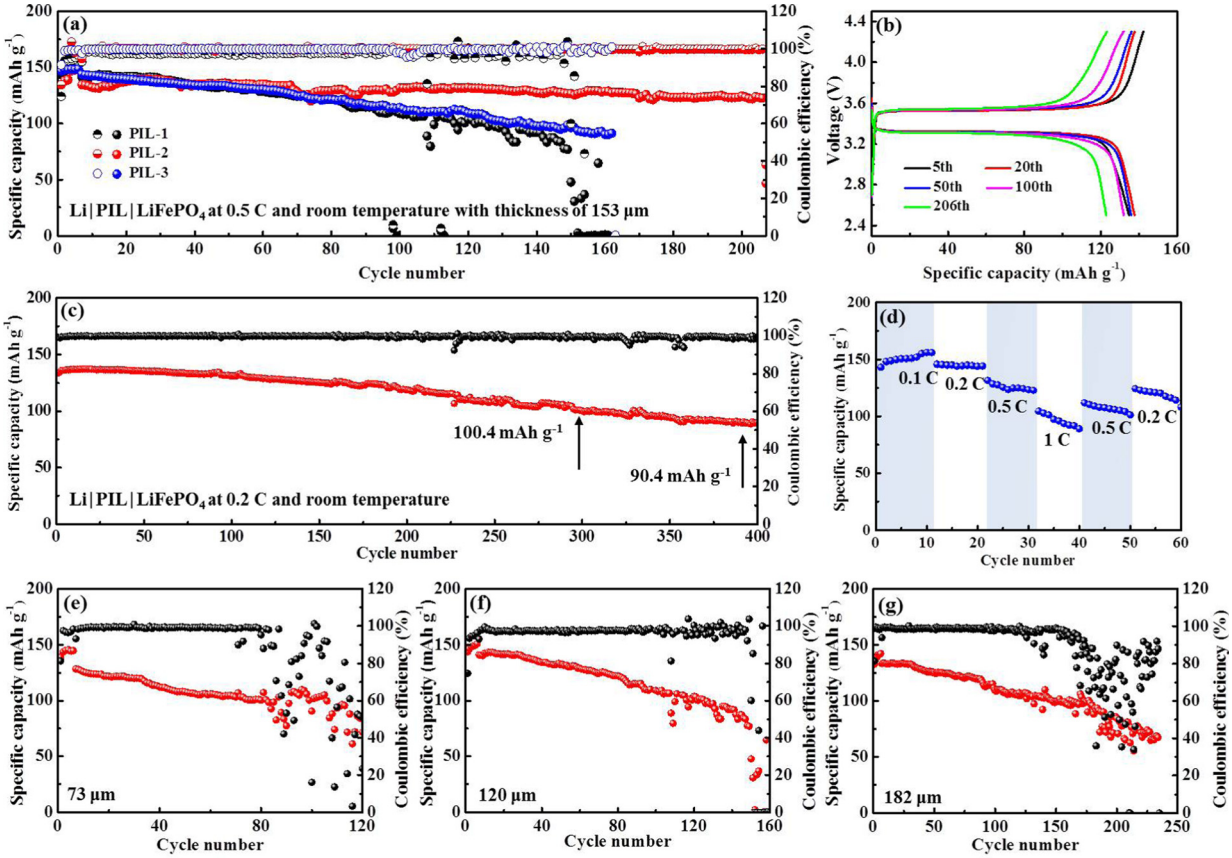

Fig. 6 Electrochemical performance of Li|PIL|LFP batteries at ambient temperature: (a), (e)–(g) with various PIL thicknesses at 0.5C, (b) typical charge/discharge profiles with the PIL thickness of 153 μm at 0.5C, (c) cycling performance at 0.2C, (d) rate performance.

the two. By definition, the ionic conductivity is inversely proportional to the thickness of the polymer membrane, the value of which descends accompanied by an increase in thickness. The SSEs with minimized thickness not only lower the battery impedance, but also make the energy density of batteries soar.[51] However, minimizing the thickness of the polymer membrane correlates with increased risk for internal short-circuit caused by the mechanical failure of SSEs. Therefore, a compromise between depleting the thickness and maintaining the mechanical strength of SSEs needs to be found. To get the critical thickness, we compare the cycling stability of Li|LFP batteries with the PIL thickness of 73, 120, 153, and 182 μm at room temperature (25 °C) and 0.5C, respectively. Notably, the Li|LFP battery with a membrane thickness of 153 μm exhibits optimum capacity retention and cyclic life (Fig. 6(e)–(g)), which presents CE (Coulombic efficiency) of 81% in the initial cycle and quickly stabilizes at ~100% without instability. As a comparison, for a battery with a membrane thickness of 73 μm, the CE delivers a fluctuating and irregularly varying pattern after maintaining itself at ~99% over 80 cycles, implying severe parasitic reactions and irreversible Li consumption due to inferior interface stableness. The same phenomenon happens to the batteries with the membrane thickness of 120 and 182 μm after 150 and 170 cycles, respectively.

Inspired by the desirable cyclability performance realized at room temperature, we further explore the high-temperature performance (48 °C) of this battery system at 0.5C. As presented in Fig. 7(a) and (b), the long-term capacity retention is markedly enhanced. For the batteries with a membrane thickness of 120 and 153 μm, a much more prolonged lifespan is achieved. Especially for the latter, the battery can be cycled up to 560 cycles, maintaining 74.5% capacity retention with a stabilized CE of almost 100%. On the contrary, batteries with a membrane thickness of 73 and 182 μm suffer from rapid decay in capacity. The photograph in Fig. 7(c) illustrates that both LFP and Li electrodes are intimately embedded into the sticky PIL membrane, rendering an integrated electrode/electrolyte interface. No obvious dividing line can be found to distinguish the solid electrolyte from electrodes (Fig. 7(d)). After cycling, there is no clear variation observed on the membrane surface in Fig. 7(e), indicating its inertness to high-temperature processing. The outcome manifests that the polymer electrolyte is well-compatible with the electrodes. Table 1 and Table S3 (ESI†) compare the critical features and electrochemical performance of the PIL electrolyte with recently reported various electrolytes conceived for LMBs. The comparison not only shows the outstanding ionic conductivity of the PIL electrolyte, but also explicitly presents the remarkable

Published on 19 2022. Downloaded on 16.10.2025 08:37:42.

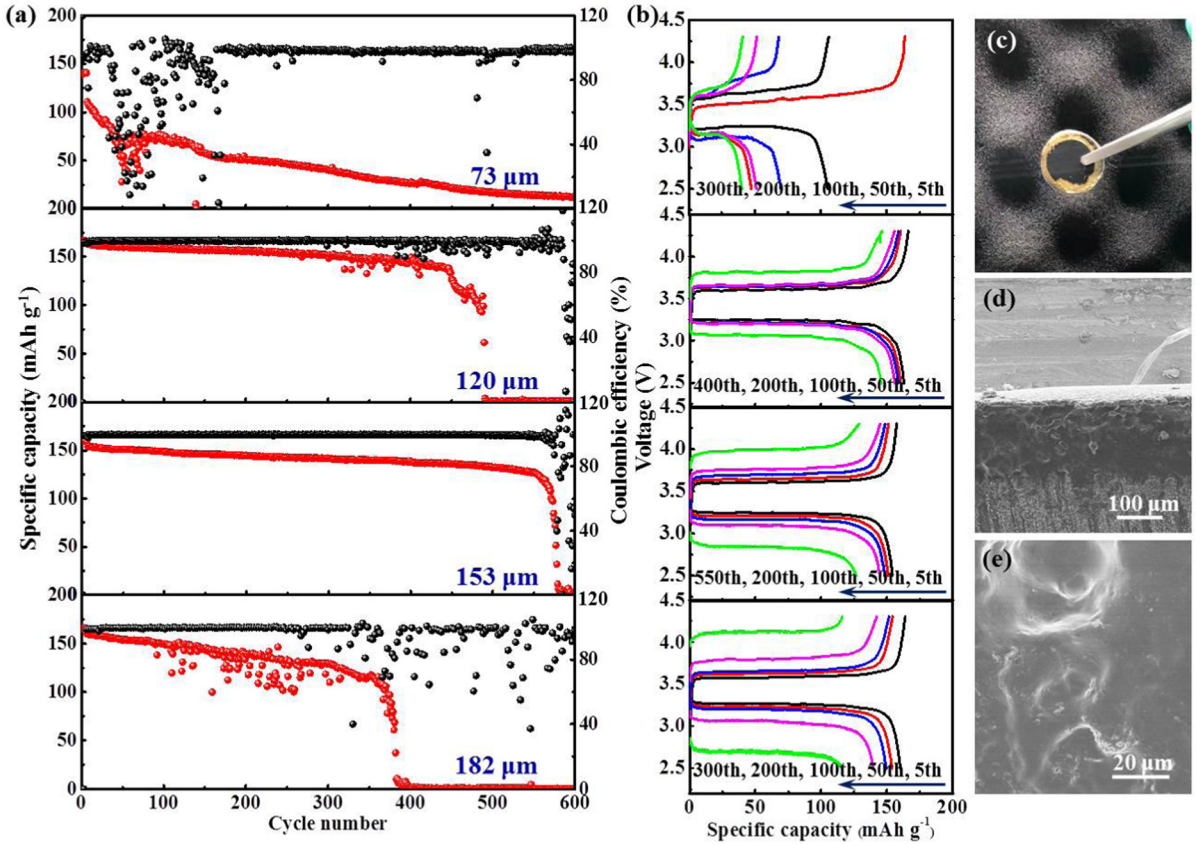

Fig. 7 (a and b) High-temperature performances (48 °C) of Li|LFP batteries using PIL membranes with various thicknesses; (c) digital photo of PIL-based Li|LFP battery after cycling; (d) cross-sectional SEM image of the cycled battery; (e) top-view SEM image of PIL membrane after cycling.

Table 1 Comparison of the critical features of PIL electrolytes with different polymer electrolytes

Polymer electrolyte	Ionic conductivity/ $\times 10^{-4}$ S cm^{-1}	Operating temperature	Capacity retention	Test rate	Cycling performance based on Li/LiFePO$_4$ batteries
EMIMTFSI/P(MMA-*co*-AMIMTFSI)[25]	1.9 at 25 °C	25 °C	65.5%	0.2C	76.3 mA h g^{-1} after 90 cycles
PEO networks crosslinked by imine and disulfide bonds[27]	6.97 at 25 °C	25 °C	88.4%	0.1C	128.5 mA h g^{-1} after 300 cycles
EMITFSI-poly(C1-4TFSI)-PDDATFSI[34]	10.6 at 25 °C	25 °C	97.7%	0.1C	147.1 mA h g^{-1} after 100 cycles
TEOS in PAN[38]	4.3 at 20 °C	25 °C	84.7%	0.5C	114.9 mA h g^{-1} after 400 cycles
XVIm-TFSI-PEGDME[41]	>1.0 at 25 °C	25 °C	93.8%	0.2C	155.0 mA h g^{-1} after 150 cycles
FB-SPE (PEGMA-HFBMA)[42]	1.45 at 70 °C	70 °C	96%	0.1C	101.7 mA h g^{-1} after 60 cycles
Br-modified cellulose-Li salt-PEGA[43]	0.35 at 25 °C	60 °C	91.8%	0.1C	134.8 mA h g^{-1} after 110 cycles
PVDF-HFP-MPEGA-ETPTA-Pyr$_{13}$TFSI-HMPP-LiTFSI[52]	11.9 at 25 °C	55 °C	98.3%	0.5C	148.5 mA h g^{-1} after 200 cycles
PSi-S-CN-DMPA[53]	0.045 at 25 °C	60 °C	75%	0.1 mA cm^{-2}	100.5 mA h g^{-1} after 150 cycles
PEO-Pyr$_{1,(2O)7}$TFSI-LiTFSI[54]	6.6 at 25 °C	40 °C	99.3%	1C	151 mA h g^{-1} after 200 cycles
LATP-LiTFSI-Py$_{13}$TFSI-PDADMATFSI[55]	1.03 at 40 °C	50 °C	95%	0.1C	166.25 mA h g^{-1} after 100 cycles
Poly(allyl diglycol carbonate)[56]	0.196 at 25 °C	60 °C	99.2%	0.3C	127.4 mA h g^{-1} after 110 cycles
EMIm-TFSI in cross-linking EPVIm-TFSI/PEI/PVDF-HFP network[57]	18 at 25 °C	25 °C	98%	0.5C	147.5 mA h g^{-1} after 200 cycles
Polymerized 1,3-dioxolane[58]	33.7 at 25 °C	25 °C	82.1%	100 mA g^{-1} ~2.3C	115 mA h g^{-1} after 200 cycles
UPyMA-PEGMA-SSPSILi/PVDF-HFP[59]	0.278 at 30 °C	25 °C	93.6%	0.1C	105 mA h g^{-1} after 100 cycles
BC-*g*-PLiSTFSI-*b*-PEGM[60]	3.1 at 25 °C	25 °C	~84%	0.5C	111 mA h g^{-1} after 300 cycles
Crosslinked PEGDE[61]	0.89 at 25 °C	25 °C	74.2%	0.1C	95 mA h g^{-1} after 100 cycles
SnF_2 catalyzed P-DOL[62]	0.72 at 45 °C	45 °C	81.8%	0.15C	130 mA h g^{-1} after 350 cycles
Our work	1.76 at 25 °C	25 °C	91.2%	0.5C	119.9 mA h g^{-1} after 206 cycles
		25 °C	67.6%	0.2C	90.4 mA h g^{-1} after 392 cycles
		48 °C	74.5%	0.5C	146.1 mA h g^{-1} after 560 cycles

thermal endurance, oxidative stability, and easy device integration. In consideration of these excellent traits, the PIL electrolyte is highlighted as a strong competitor for use in high-energy-density solid-state LMBs.

 This journal is © The Royal Society of Chemistry 2023

Published on 19 2022. Downloaded on 16.10.2025 08:37:42.

3. Conclusion

In conclusion, we introduced a new type of polymer electrolyte by grafting $EMIM^+$ into the backbones of PMMA polymer, imparting chemical inertness against the Li anode, which is a characteristic of high Li^+ transport and self-healing traits. Benefiting from the strong external H-bonding interactions, the obtained polymer electrolyte could spontaneously reconstruct dendrite-induced defects and fatigue crack growth at the Li/electrolyte interface, giving rise to uniform Li deposition. Owing to the resilient Li/electrolyte interface and dendrite-free Li plating, the Li|LFP batteries with self-healing polymer electrolyte display an optimal initial discharge capacity of 134.7 mA h g^{-1}, rendering 91.2% capacity retention after 206 cycles at room temperature. When the operating temperature was raised to 48 °C, the battery could be cycled up to 560 cycles, maintaining 74.5% capacity retention with a stabilized CE of almost 100%. All the results illustrate the competitive advantages of the self-healing polymer for practical LMBs with highly improved safety and interfacial stability.

Conflicts of interest

There are no conflicts to declare.

Acknowledgements

The work is financially supported by the NSFC (21905141, 22203046, 91963119, 22179064, 62174087), China Postdoctoral Science Foundation (2020M681682), Priority Academic Program Development of Jiangsu Higher Education Institutions (YX03001), Synergetic Innovation Centre for Organic Electronics and Information Displays, and Jiangsu National Synergetic Innovation Centre for Advanced Materials (SICAM). The authors would like to thank Shiyanjia Lab (www.shiyanjia.com) for conducting the GPC tests.

References

1 D. C. Lin, Y. Y. Liu and Y. Cui, *Nat. Nanotechnol.*, 2017, **12**, 194–206.
2 Y. Cao, H. M. Lu, B. B. Xu, W. W. Yang and Q. S. Hong, *Chem. Eng. J.*, 2019, **378**, 122247.
3 Q. Wang, H. C. Wang, J. Y. Wu, M. Y. Zhou, W. Liu and H. H. Zhou, *Nano Energy*, 2021, **80**, 105516.
4 Z. D. Hao, Q. Zhao, J. D. Tang, Q. Q. Zhang, J. B. Liu, Y. H. Jin and H. Wang, *Mater. Horiz.*, 2021, **8**, 12–32.
5 R. Gond, W. V. Ekeren, R. Mogensen, A. J. Naylor and R. Younesi, *Mater. Horiz.*, 2021, **8**, 2913–2928.
6 L. S. Su, A. Manthiram and A. Manthiram, *Small Struct.*, 2022, 2200114.
7 P. Liu, H. Su, Y. Liu, Y. Zhong, C. X. Xian, X. L. Xia, Y. Q. Zhang, X. L. Wang, X. H. Xia and J. P. Tu, *Small Struct.*, 2022, **3**, 220010.
8 Y. Liu, Y. P. Zhai, Y. Y. Xia, W. Li and D. Y. Zhao, *Small Struct.*, 2021, **2**, 2000118.
9 H. Liu, X. B. Cheng, J. Q. Huang, H. Yuan, Y. Lu, C. Yan, G. L. Zhu, R. Xu, C. Z. Zhao, L. P. Hou, C. X. He, S. Kaskel and Q. Zhang, *ACS Energy Lett.*, 2020, **5**, 833–843.
10 M. Balaish, J. C. Gonzalez-Rosillo, K. J. Kim, Y. T. Zhu, Z. D. Hood and J. L. M. Rupp, *Nat. Energy*, 2021, **6**, 227–239.
11 X. L. Xu, K. S. Hui, K. N. Hui, H. Wang and J. B. Liu, *Mater. Horiz.*, 2020, **7**, 1246–1278.
12 A. Manthiram, X. W. Yu and S. F. Wang, *Nat. Rev.*, 2017, **2**, 16103.
13 Y. Cao, H. M. Lu, Q. S. Hong, J. J. Bai, J. R. Wang and X. D. Li, *J. Power Sources*, 2017, **368**(15), 78–87.
14 Y. Cao, H. M. Lu, Q. S. Hong, B. B. Xu, J. R. Wang, Y. Deng, W. W. Yang and W. Cai, *Carbon*, 2019, **144**, 280–288.
15 W. R. Du, X. F. Du, M. B. Ma, S. Huang, X. F. Sun and L. L. Xiong, *Adv. Funct. Mater.*, 2022, **32**, 2110871.
16 N. Meng, F. Lian and G. L. Cui, *Small*, 2021, **17**, 2005762.
17 W. W. Yang, H. M. Lu, Y. Cao and P. C. Jing, *J. Power Sources*, 2019, **441**, 227173.
18 D. P. Wang, S. F. Zhao, R. Y. Yin, L. L. Li, Z. Lou and G. Z. Shen, *npj Flexible Electron.*, 2021, **5**, 13.
19 M. R. Crump, S. L. Bidinger, F. J. Pavinatto, A. T. Gong, R. M. Sweet and J. D. MacKenzie, *npj Flexible Electron.*, 2021, **5**, 7.
20 M. H. Kim, H. L. Park, M. H. Kim, J. Jang, J. H. Bae, I. M. Kang and S. H. Lee, *npj Flexible Electron.*, 2021, **5**, 34.
21 J. Hwang, K. Matsumoto, C. Y. Chen and R. Hagiwara, *Energy Environ. Sci.*, 2021, **14**, 5834–5863.
22 C. Y. Fu, G. Homann, R. Grissa, D. Rentsch, W. G. Zhao, T. Gouveia, A. Falgayrat, R. Y. Lin, S. Fantini and C. Battaglia, *Adv. Energy Mater.*, 2022, **12**, 2200412.
23 J. Zhang, Z. Y. Chen, Y. Zhang, S. Y. Dong, Y. F. Chen and S. G. Zhang, *Adv. Mater.*, 2021, **33**, 2100962.
24 Z. H. Luo, W. J. Li, J. P. Yan and J. Sun, *Adv. Funct. Mater.*, 2022, **32**, 2203988.
25 C. X. Guo, Y. F. Cao, J. F. Li, H. P. Li, S. K. Arumugam, S. Oleksandr and F. Chen, *Appl. Energy*, 2022, **323**, 119571.
26 Z. Li, J. L. Fu, S. Zheng, D. G. Li and X. Guo, *Small*, 2022, **18**, 2200891.
27 Z. X. Huang, Z. H. Xie, Z. P. Zhang, T. Zhang, M. Z. Rong and M. Q. Zhang, *J. Mater. Chem. A*, 2022, **10**, 18895–18906.
28 X. Lin, X. Liu, S. Xu, Z. Liu, C. Zhao, R. Liu, P. Li, X. Feng and Y. Ma, *New J. Chem.*, 2022, **46**, 10379–10385.
29 S. Z. Wang, J. W. Hu, X. F. Gui, S. D. Lin and Y. Y. Tu, *J. Electrochem. Soc.*, 2021, **168**, 020514.
30 S. F. Xiang, S. S. Chen, M. T. Yao, F. Zheng and Q. H. Lu, *J. Mater. Chem. C*, 2019, **7**, 9625–9632.
31 B. Yu, F. Zhou, C. W. Wang and W. M. Liu, *Eur. Polym. J.*, 2007, **43**, 2699–2707.
32 S. J. Ding, H. D. Tang, M. Radosz and Y. Q. Shen, *Polym. Chem.*, 2004, **42**, 5794–5801.
33 T. H. Zhou, Y. Zhao, J. W. Choi and A. Coskun, *Angew. Chem., Int. Ed.*, 2021, **60**, 22791–22796.
34 D. Zhou, R. L. Liu, J. Zhang, X. G. Qi, Y. B. He, B. H. Li, Q. H. Yang, Y. S. Hu and F. Y. Kang, *Nano Energy*, 2017, **33**, 45–54.
35 S. Hess, M. Wohlfahrt-Mehrens and M. Wachtler, *J. Electrochem. Soc.*, 2015, **162**, A3084.

Published on 19 2022. Downloaded on 16.10.2025 08:37:42.

36 Q. Liu, D. Zhu, D. Shanmukaraj, P. Li, F. Y. Kang, B. H. Li, M. Armand and G. X. Wang, *ACS Energy Lett.*, 2020, **5**, 1456–1464.
37 K. Q. He, S. H. Cheng, J. Y. Hu, Y. Q. Zhang, H. W. Yang, Y. Y. Liu, W. C. Liao, D. Z. Chen, C. Z. Liao, X. Cheng, Z. G. Lu, J. He, J. N. Tang, R. K. Y. Li and C. Liu, *Angew. Chem., Int. Ed.*, 2021, **60**, 12116–12123.
38 M. Yao, H. T. Zhang, C. X. Xing, Q. G. Li, Y. J. Tang, F. J. Zhang, K. Yang and S. J. Zhang, *Energy Storage Mater.*, 2021, **41**, 51–60.
39 K. Pożyczka, M. Marzantowicz, J. R. Dygas and F. Krok, *Electrochim. Acta*, 2017, **227**, 127–135.
40 H. Kim, W. Choi, J. Yoon, J. H. Um, W. Lee, J. Kim, J. Cabana and W. S. Yoon, *Chem. Rev.*, 2020, **120**, 6934–6976.
41 Y. C. Tseng, S. H. Hsiang, C. H. Tsao, H. Teng, S. S. Hou and J. S. Jan, *J. Mater. Chem. A*, 2021, **9**, 5796–5806.
42 M. Y. Jia, P. Wen, Z. T. Wang, Y. C. Zhao, Y. M. Liu, J. Lin, M. Chen and X. R. Lin, *Adv. Funct. Mater.*, 2021, 2101736.
43 Y. Zhang, L. P. Yu, J. R. Wang, S. Q. Li, H. H. Gan and Z. G. Xue, *J. Membr. Sci.*, 2021, **626**, 119210.
44 J. Tan, J. Matz, P. Dong, J. F. Shen and M. X. Ye, *Adv. Energy Mater.*, 2021, **11**, 2100046.
45 P. Jaumaux, Q. Liu, D. Zhang, X. F. Xu, T. Y. Wang, Y. Z. Wang, F. Y. Kang, B. H. Li and G. X. Wang, *Angew. Chem., Int. Ed.*, 2020, **59**, 9134–9143.
46 C. Y. Chang, Y. Yao, R. R. Li, Z. H. Guo, L. W. Li, C. X. Pan, W. G. Hu and X. Pu, *Nano Energy*, 2022, **93**, 106871.
47 W. W. Yang, H. M. Lu, Y. Cao, P. C. Jing, X. Q. Hu and H. Yu, *Ionics*, 2020, **26**, 3405–3413.
48 W. W. Yang, H. M. Lu, Y. Cao, B. B. Xu, Y. Deng and W. Cai, *ACS Sustainable Chem. Eng.*, 2019, **7**, 4861–4867.
49 J. X. Liu, C. Zhang, S. Q. Yuan, W. W. Yang, Y. Cao, J. Y. Deng, B. B. Xu and H. M. Lu, *Chem. Eng. J.*, 2022, **428**, 131326.
50 Z. Zhang, Y. Huang, H. Gao, C. Li, J. X. Hang and P. B. Liu, *J. Energy Chem.*, 2021, **60**, 259–271.
51 J. Y. Wu, L. X. Yuan, W. X. Zhang, Z. Li, X. L. Xie and Y. H. Huang, *Energy Environ. Sci.*, 2021, **14**, 12–36.
52 Z. Chen, Y. Yang, Q. T. Su, S. D. Huang, D. Song, R. Ma, C. Z. Zhu, G. H. Lv and C. H. Li, *ACS Appl. Mater. Interfaces*, 2021, **13**, 41946–41955.
53 C. Y. Fu, M. Iacob, Y. Sheima, C. Battaglia, L. Duchêne, L. Seidl, D. M. Opris and A. Remhof, *J. Mater. Chem. A*, 2021, **9**, 11794–11801.
54 J. Atik, D. Diddens, J. H. Thienenkamp, G. Brunklaus, M. Winter and E. Paillard, *Angew. Chem., Int. Ed.*, 2021, **60**, 11919–11927.
55 X. L. Song, H. T. Zhang, D. F. Jiang, L. P. Yang, J. H. Zhang, M. Yao, X. Y. Ji, G. Y. Wang and S. J. Zhang, *Electrochim. Acta*, 2021, **368**, 137581.
56 Y. B. Chen, G. P. Chen, C. Q. Niu, W. Y. Shang, R. T. Yu, C. X. Fang, P. Ouyang and J. Du, *Polymer*, 2021, **223**, 123695.
57 L. Liang, X. H. Chen, W. F. Yuan, H. Chen, H. Y. Liao and Y. Q. Zhang, *ACS Appl. Mater. Interfaces*, 2021, **13**, 25410–25420.
58 S. S. Wang, L. Zhou, M. K. Tufail, L. Yang, P. F. Zhai, R. J. Chen and W. Yang, *Chem. Eng. J.*, 2021, **415**, 128846.
59 H. H. Gan, S. Q. Li, Y. Zhang, L. P. Yu, J. R. Wang and Z. G. Xue, *Langmuir*, 2021, **37**, 8270–8280.
60 M. H. Zhou, R. L. Liu, D. Y. Jia, Y. Cui, Q. T. Liu, S. H. Liu and D. C. Wu, *Adv. Mater.*, 2021, **33**, 2100943.
61 Y. Y. Cui, X. M. Liang, J. C. Chai, Z. L. Cui, Q. L. Wang, W. S. He, X. C. Liu, Z. H. Liu, G. L. Cui and J. W. Feng, *Adv. Sci.*, 2017, **4**, 1700174.
62 W. Li, J. Gao, H. Y. Tian, X. L. Li, S. He, J. P. Li, W. L. Wang, L. Li, H. Li, J. S. Qiu and W. D. Zhou, *Angew. Chem., Int. Ed.*, 2022, **134**, e202114805.

 This journal is © The Royal Society of Chemistry 2023